Title

Fast in vivo 23Na imaging and mapping using accelerated 2D-FID UTE magnetic resonance spectroscopic imaging at 3 T: Proof of concept and reliability study

Journal

Magnetic Resonance in Medicine, 85(4)

ISSN

0740-3194

Authors

Alhulail, Ahmad A
Xia, Pingyu
Shen, Xin
et al.

Publication Date

2021-04-01

DOI

10.1002/mrm.28576

Peer reviewed

HHS Public Access

Author manuscript

Magn Reson Med. Author manuscript; available in PMC 2022 April 01.

Published in final edited form as:

Magn Reson Med. 2021 April ; 85(4): 1783–1794. doi:10.1002/mrm.28576.

Fast in vivo ^{23}Na imaging and T_2* mapping using accelerated 2D-FID UTE magnetic resonance spectroscopic imaging at 3 T: Proof of concept and reliability study

Ahmad A. Alhulail[1,2], **Pingyu Xia**[1], **Xin Shen**[3], **Miranda Nichols**[1], **Srijyotsna Volety**[1], **Nicholas Farley**[1], **M. Albert Thomas**[4], **Armin M Nagel**[5,6], **Ulrike Dydak**[1,7], **Uzay E. Emir**[1,3]

[1]School of Health Sciences, Purdue University, West Lafayette, Indiana

[2]Department of Radiology and Medical Imaging, Prince Sattam bin Abdulaziz University College of Applied Medical Sciences, Al Kharj, Saudi Arabia

[3]Weldon School of Biomedical Engineering, Purdue University, West Lafayette, Indiana

[4]Department of Radiology, University of California Los Angeles, Los Angeles, California

[5]Institute of Radiology, University Hospital Erlangen, Friedrich-Alexander-Universität Erlangen-Nürnberg (FAU), Erlangen, Germany

[6]Division of Medical Physics in Radiology, German Cancer Research Center (DKFZ), Heidelberg, Germany

[7]Department of Radiology and Imaging Sciences, Indiana University School of Medicine, Indianapolis, Indiana

Abstract

Purpose: To implement an accelerated MR-acquisition method allowing to map T_2* relaxation and absolute concentration of sodium within skeletal muscles at 3T.

Methods: A fast-UTE-2D density-weighted concentric-ring-trajectory ^{23}Na-MRSI technique was used to acquire 64 time-points of FID with a spectral bandwidth of 312.5 Hz with an in-plane resolution of 2.5 × 2.5 mm^2 in about 15 minutes. The fast-relaxing ^{23}Na signal was localized with a single-shot, inversion-recovery based, non-echo (SIRENE) OVS method. The sequence was verified using simulation and phantom studies before implementing it in human-calf muscles. To evaluate the 2D-SIRENE-MRSI (UTE = 0.55 ms) imaging performance, it was compared to a 3D-MRI (UTE = 0.3 ms) sequence. Both datasets were acquired within two same-day sessions to assess repeatability. The T_2* values were fitted voxel-by-voxel using a bi-exponential model for the 2D-MRSI data. Finally, intra-subject coefficients of variation (CV) were estimated.

Results: The MRSI-FID data allowed us to map the fast and slow components of T_2* in the calf muscles. The spatial-distributions of ^{23}Na concentration for both MRSI and 3D-MRI acquisitions

Correspondence: Uzay Emir, School of Health Sciences, Purdue University, School of Health Sciences, 550 Stadium Mall Drive, West Lafayette, IN 47907. uemir@purdue.edu.

SUPPORTING INFORMATION

Additional supporting information may be found online in the Supporting Information section at the end of this article.

were significantly correlated (P<0.001). The test-retest analysis rendered high repeatability for MRSI with a CV of 5%. The mean T^*_{2Fast} in muscles was 0.7 ± 0.1 ms (contribution fraction = 37%), while T^*_{2Slow} was 13.2 ± 0.2 ms (63%). The mean absolute muscle ^{23}Na concentration calculated from the T_2*-corrected data was 28.6 ± 3.3 mM.

Conclusion: The proposed MRSI technique is a reliable technique to map sodium's absolute concentration and T_2* within a clinically acceptable scan time at 3T.

Keywords

sodium; MRSI; fast; T_2 mapping; OVS localization; skeletal muscles; quantification

1 | INTRODUCTION

Sodium (^{23}Na) plays a crucial role in preserving many vital functions in our bodies. Under healthy conditions, ^{23}Na concentration stays within certain ranges but varies among tissue types.[1] The alterations in these ranges might be a sign of health disorder or physiological changes. In skeletal muscles, the increase in ^{23}Na concentration was used as a biochemical marker for several diseases such as hypertension[2], diabetes,[3] or muscular channelopathies.[4,5] It was also used for monitoring early therapeutic responses.[6] The physiological changes due to exercise have also been observed by using ^{23}Na-MR. An increase in muscle sodium concentration has been noticed after the exercises.[7] In a similar study, this has been suggested to be a result of an increase in the transverse relaxation time (T_2).[8]

^{23}Na possesses 3/2 nuclear spin and its relaxation is determined by the quadrupolar interaction (QI = the interaction between the ^{23}Na nuclear quadrupole moment and the local electric field gradients), and the containing environment.[9,10] In an aqueous solution, the time-averaged QI equals to zero, and the spins move freely and tumble very fast. Subsequently, ^{23}Na exhibits a relatively long monoexponential T_2. However, within a biological system, ^{23}Na spins interact with the surrounding macromolecules, and a time averaged QI ≠ 0 is possible. As the mobility of ^{23}Na gets more restricted, the transverse relaxation becomes biexponential.[10] The monoexponential relaxation decay within in-vitro aqueous ^{23}Na solutions is ranging between 20–50 ms.[11,12] A monoexponential ^{23}Na relaxation of 55–65 ms was only reported for the CSF.[1,13] In human muscles, the fast transverse relaxation time (T^*_{2Fast}) ranges between 0.5–3.0 ms, whereas slow transverse relaxation time (T^*_{2Slow}) ranges between 12–28.[14] This variation in relaxation modes and magnitude between the in-vivo and in-vitro environments can result in a quantification bias. Similarly, the longitudinal relaxation time (T_1) of ^{23}Na is short. At 3T, the T_1 of ^{23}Na in skeletal muscles has been estimated to be about 29 ms.[4] Thus, a careful relaxation measurement is necessary to conduct accurate quantification studies yielding useful physiological information.

Sodium T_2* mapping and absolute quantification suffer from several challenges originating from lower intrinsic SNR and shorter T_2* relaxation values compared with ^{1}H.[1,14] Thus, to overcome these issues, measurements at ultra-short TE (UTE), increasing the voxel size, taking more averages, and/or scan with ultra-high magnetic fields > 3T have been proposed.

[7,13,15–22] Increasing voxel dimensions will be at the expense of large partial-volume artifacts. Alternatively, taking more averages will lengthen the scan duration. 3D MRI methods have been the method of choice to increase SNR and reduce the echo time since it does not require any slice selection. In addition, estimation of the relaxation times and correcting for relaxation effects can further improve the quantitative accuracy. However, this requires acquiring multiple-echo data to perform T_2* with a cost of prolonged acquisition time.

While the 3D-MRI technique is the common method to capture the T^*_{2Fast}, conducting relaxometry studies require impractical acquisition scan duration.[13,15–20] The used ^{23}Na-relaxometry techniques suffer either from a limitation in their spatial precision (large voxel covering different tissue types) or from their impractical acquisition time. The T_2* values of intact skeletal muscles have been measured previously using non-localized FID methods.[8,21] Such relaxometry methods estimate the averaged value from a large scanned area, which may include different tissues in addition to the muscles. To conduct the relaxometry study with a better spatial resolution, a 3D-UTE acquisition technique has been used with images acquired at different echo times, which consumes a long scan time (9 min per echo), and with a coarse in-plane spatial resolution (6 × 6 mm^2).[7] Alternatively, a multi-echo GRE sequence has been used to measure the T_2* over the entire slice of interest with higher resolution and shorter total time (~14 minutes).[22] However, since GRE starts with a slice-selective gradient, the minimum possible first echo was 1.9 ms, which may not be short enough to detect the fast decaying component of the T_2*. To allow shorter TEs and avoid the lengthy slice-selective gradients, outer volume suppression (OVS) methods such as single-shot, inversion-recovery based, non-echo (SIRENE)[23] and FIDLOVS[24] have been proposed. However, these methods have not been applied and tested for ^{23}Na imaging.

Therefore, the goal of this work was to develop an accelerated method with an early acquisition start to estimate in vivo T_2* values of muscle tissues in a voxel-wise manner at 3T while maintaining high spatial and temporal resolution. To attain this, we are proposing an accelerated density-weighted concentric ring trajectory (DW-CRT) MRSI acquisition to measure in vivo ^{23}Na relaxation times in the lower leg muscles with a high sampling frequency. Additionally, to mitigate the long TE limitation when using slice-selective gradients, the SIRENE method[23] was used instead to reach UTE. Before conducting an in-vivo repeatability study, the localization method was tested using simulation and in-vitro experiments. Additionally, to validate the imaging ability of our proposed MRSI, we will compare its results to images acquired by a state-of-the-art UTE-3D-MRI sequence. This comparison would also help us to evaluate the importance of performing T_2* correction.

2 | METHODS

2.1 | Sequence design

The sequence begins with a pair of slice-selective gradients and adiabatic full passage inversion pulses (hyperbolic secant (HS20) pulses, B_1 peak of 19.2 μT, a pulse duration of 12.8 ms, and a thickness of 100 mm) to invert the magnetization bands outside the desired slice of interest (SOI) along the z direction and followed by spoiler gradients. After a delay

chosen to null the inverted magnetization (TI = ln[2] × tissue's T_1, 20 ms in our case), pairs of wide-bandwidth adiabatic half passage OVS saturation pulses (HS20, B_1 peak of 29 μT, a pulse duration of 2.56 ms, and thickness of 100 mm) and gradients along z-axis were applied. The net effect is to eliminate the magnetization within the bands at each side of the SOI. The FID is then measured from the remaining magnetization within the SOI after a square excitation pulse with a duration of 240 μs (Figure 1). To accelerate data collection, the k-space data is collected by using a fast density-weighted concentric ring trajectory (DW-CRT) acquisition similar to that implemented in Chiew et al.[25]

2.2 | Outer volume suppression bands performance evaluation

2.2.1 | Simulation—The performance of the OVS bands for eliminating the entire ^{23}Na signal outside the SOI was evaluated by simulation using SpinBench software (HeartVista, Inc. Menlo Park, CA). The identical MRSI experimental parameters were used for the simulation software together with the approximated skeletal muscle sodium NMR properties at 3T (gyromagnetic ratio = 11.25 MHz/T, T_1 = 29 ms, fast T_2* = 0.5 ms, and slow T_2* = 12 ms). The resulted thickness, sharpness, and residual signal amplitude over the generated spatial profile were used to judge and optimize the bands' parameters (Figure 2A).

2.2.2 | Phantom experiment—To test the optimized OVS bands parameters on the scanner, a phantom study was conducted. Four phantoms (bottles) were prepared with different known ^{23}Na concentrations (10, 20, 30, 40 mM), which will also serve as a calibration reference for the in vivo signal quantification. To achieve the in-vivo T_1 of sodium, 2.9 g/L $CuSO_4$ was added to each phantom.

To ensure that no signal is coming from outside the SOI, a scan was acquired while two ^{23}Na phantoms of the highest concentration (30 and 40 mM) were placed outside the SOI, within the OVS bands. The remaining phantoms of lower concentration (10 and 20 mM) were placed in the center of the SOI (Figure 2B). For comparison, ^{23}Na images with a 3D-MRI scan covering the same SOI were also acquired.

2.3 | In vivo experiment

2.3.1 | Human subjects—In vivo calf muscle scans were performed in four subjects [1 male and 3 females; age 22–40 years (median = 26 years); body mass index (BMI) = 24 ± 3 kg/m^2]. The study was conducted in accordance with the institutional review board of Purdue University. Before being scanned, an informed written consent was obtained from all the subjects.

2.3.2 | Repeatability study—In order to evaluate the reliability of the proposed MRSI method, test-retest scans were performed. The subjects were asked to lie in a feet-first supine position with their left leg within a ^{23}Na coil. The maximum circumference of their lower leg was positioned to be centered in the middle of the coil. Additionally, to make sure that both scans were acquired from the same slice, an ink marker was used to draw a line on the leg region (~10.5–11.5 cm below the knee joint, based on the subject) where the scanner laser marker was centered for the first scan. After a short break (about 5 minutes) outside of the scanner, the repeat scan was acquired using the same scanning protocol.

2.3.3 | Scanning parameters—The data were collected using a 3T Siemens Prisma MR system (Siemens Healthineers, Germany) and a frequency-tuned mono-resonant ^{23}Na-transmit/receive birdcage knee coil (32.6 MHz, Stark-Contrast, Erlangen, Germany).

The ^{23}Na data were measured through the default shim currents of the MR system ("Tune Up" under shim settings).

For the ^{23}Na-MRSI study, inversion pulses with TI of 20 ms were applied and followed by the two OVS pulses on the z-direction before the excitation RF pulse. The FID DW-CRT MRSI was implemented with an alpha of 1. The alpha parameter controls the spatial response function, and alpha = 1 was found to be providing a higher SNR with a cost of degrading the spatial response function, as described in Chiew et al.[25]. The following parameters were used for the DW-CRT MRSI: matrix size = 96 × 96, field of view (FOV) = 240 × 240 mm^2, resolution = 2.5 × 2.5 × 20 mm^3 (nominal resolution = 0.125 mL), flip angle (FA) = 90°, acquisition delay (time from the center of excitation pulse to the first FID time point) = 0.55 ms, repetition time (TR) = 650 ms, temporal samples = 64, number of rings = 48, points-per-ring = 64, spectral bandwidth = 312.5 Hz, spatial interleaves = 4, and readout duration = 204.8 ms. The scan performed with 8 averages, which resulted in a total acquisition time (TA) of 15 minutes and 24 seconds.

To evaluate the spatial mapping performance of the ^{23}Na-MRSI technique, ^{23}Na-MRI data were collected with a density-adapted 3D radial acquisition sequence[26] with UTE = 0.3 ms, TR = 100 ms, FA = 90°, 1 average, 4 × 4 × 4 mm^3 nominal resolution, and FOV = 256 × 256 mm^2, and TA = 6.66 min. Five axial slices were averaged to cover the same MRSI slice. These 3D-UTE MRI images will serve as a reference to assess the spatial distribution of the MRSI maps. It will also be used to compare the quantification results from data acquired with UTE and T_2*-corrected methods.

For segmentation, high-resolution anatomical images were acquired using the integrated body coil with a T_1-FLASH sequence of TR/TE = 250 ms/2.46 ms, FA = 60°, 2 averages, 0.6 × 0.6 × 10 mm^3 resolution, and FOV = 200 × 200 mm^2.

All the above sequences were planned to collect data from the same axial slice placed at the isocenter. Additionally, shimming using the ^{1}H coil was done before the sodium measurements.

2.3.4 | Post-processing—The reconstruction of the MRSI data were performed in MATLAB (MathWorks, Natick, MA, USA). The gridding and the Fast Fourier Transform were done using the Nonuniform FFT (NUFFT) method.[27] In addition to the DW-CRT trajectory[25], a Hanning filter was applied in k-space for density compensation.

The B_0 inhomogeneity was corrected by calculating the ^{23}Na ΔB_0 maps as described in Gast et al.[28] Here, the ^{23}Na ΔB_0 maps were calculated based on the first two ^{23}Na-MRSI phase-unwrapped images ($\theta_{TE_2,unwrapped}$ and $\theta_{TE_1,unwrapped}$) acquired at TE_1 = 0.55 ms, and TE_2 = 3.75 ms, as follows:

$$\Delta B_0 = \frac{\theta_{TE_2,unwrapped} - \theta_{TE_1,unwrapped}}{TE_2 - TE_1} \quad (1)$$

These ΔB_0 maps were used to reconstruct field-corrected ^{23}Na-MRSI images using a fast iterative image reconstruction method.[29] An example of ΔB_0 map and correction can be found in Figure 3. Finally, we applied low rank approximations for spatial-spectral denoising (2 for space-time, and 5 for Hankel filtering) of the reconstructed ^{23}Na MRSI data.[30] An example of ^{23}Na-data without and with the low-rank denoising can be found in Supporting Figure S1.

The 3D-MRI data were reconstructed using a MATLAB tool designed for the radial sequence. To reconstruct the 3D-MRI magnitude images, the k-space data were density compensated before being re-gridded with an oversampling ratio of two using a Kaiser-Bessel kernel,[31] and Fourier transformed by a conventional fast FFT. The data were filtered with a Hanning filter.

2.3.5 | Fitting of T_2*—The acquired FID data from the leg region were fitted to a biexponential decay with a nonlinear least squares method to calculate the T^*_{2Fast} and T^*_{2Slow} relaxation time components:

$$SI_{Leg}(t) = S_{Fast} \quad e^{-t/T^*_{2Fast}} + S_{Slow} \quad e^{-t/T^*_{2Slow}} + n \quad (2)$$

Here, S_{Fast} and S_{Slow} are the contributions to the initial signal from the fast and slow components, respectively, t indicates the FID points collection time, and n represents the offset level.

The initial (undecayed) signal equals the sum of S_{Fast} and S_{Slow}. Thus, their contribution fractions were represented as:

$$F_{Fast} = \frac{S_{Fast}}{S_{Fast} \quad + S_{Slow}} \quad (3)$$

$$F_{Slow} = \frac{S_{Slow}}{S_{Fast} \quad + S_{Slow}} \quad (4)$$

For the reference bottles, *Ref*, the FID curves were fitted to a monoexponential decay:

$$SI_{Ref}(t) = S_{Ref} \quad e^{-t/T^*_{2Ref}} + n \quad (5)$$

2.3.6 | Quantification—The ^{23}Na concentration maps in mM were reconstructed by calibrating the signals of the reference bottles to their corresponding known concentrations. The resulting signal-to-concentration linear equation was used to calibrate the signals within the leg and to estimate the concentration in mM.

2.3.7 | Muscle segmentation—The high-resolution T1-weighted image was used to manually draw regions of interest (ROIs) over each of the seven main large muscles (Figure 4). The borders of these ROIs were determined by tracing the boundaries of their corresponding muscle. The ROIs were then down-sampled and co-registered to each sodium map to evaluate the ^{23}Na spatial distribution. Voxels close to the main blood vessels were avoided. The subcutaneous fat region was segmented similarly.

2.3.8 | Statistical analysis—The Spearman regression analysis was performed to assess the signal spatial distribution agreement between the two used acquisition techniques within the segmented ROIs. The MRSI signals were extrapolated to their estimated values at 0.3 ms to match the TE of 3D-MRI).

To evaluate the repeatability of the MRSI and 3D-MRI methods, coefficient of variance (CV), intraclass correlation coefficient (ICC), and Bland–Altman analyses were utilized.

3 | RESULTS

3.1 | Outer volume suppression bands performance evaluation

The result of the simulation (Figure 2A) showed that using a TI of 20 ms provides a sharp suppression profile. The spatial profile in Figure 2A represents the ^{23}Na magnetization after the 90° excitation. While the signal within the OVS bands is totally suppressed, the magnetization within the SOI has full transverse magnitude in a slice thickness of 20 mm.

In-line with the simulation, the phantom study has demonstrated that the signals from the high ^{23}Na concentration phantoms (30 and 40 mM) were totally suppressed by the OVS bands (Figure 2B). Thus, the signals of the low concentration phantoms (10 and 20 mM) within the SOI do not have any contamination and are in agreement with the 3D-MRI sequence (Figure 2B).

3.2 | In vivo experiment

The results of the biexponential T_2* values (T^*_{2Fast} and T^*_{2Slow}) and their fractions are summarized in Table 1 together with the T_2*-corrected concentration within each ROI. Fast and slow T_2*-maps and their corresponding signal fraction maps are illustrated in Figure 5. The T_2* correction was demonstrated by showing sodium maps before and after correction with their difference (Figure 6A–C). Additionally, Figure 6D shows an example of two signals with similar initial MR signals diverging with time due to their different transverse relaxation in different environments. The ^{23}Na spins decay monoexponentially within the reference phantom (blue) and biexponentially within the muscle (green).

As shown in Figure 7, the MRSI quantitative data was compared to the UTE 3D-MRI at three conditions: 1- the MRSI data at 0.55 ms, 2- extrapolated values to the 3D-MRI TE of 0.3 ms, and 3- at 0 ms using the estimated T_2* values. Before T_2* correction, the comparison slope between the 3D-MRI and MRSI was 0.88, which increased to 1 at 0.3 ms. After the T_2* correction, the comparison slope increased to 1.27. For all conditions, the regression analysis resulted in significant correlation ($P < 0.001$).

A representative set of baseline and repeated scan maps of the MRSI ^{23}Na concentration (before and after T_2* correction) and their corresponding 3D-MRI maps are provided in Figure 8. The repeatability of the muscle and subcutaneous fat ROIs from all subjects are shown in Figure 9. The CV was calculated as 4.2, 5.2, and 5.9 %, and the ICC as 0.98, 0.95, and 0.89 for the MRSI data before correction, after correction, and the 3D MRI data, respectively.

4 | DISCUSSION

In this work, we have introduced a novel method to acquire ^{23}Na 2D-FID data with short acquisition delay (0.55 ms) with a good spatial-quality comparable to a well-established 3D acquisition method. The proposed method provides additional time points in the FID to calculate both of T_2* and ΔB_0, and correct for their effects without additional scans.

To reduce the delay time while performing a 2D-measurement, we utilized a single-shot, inversion-recovery based, non-echo (SIRENE) method based on OVS bands[23]. In this study, we implemented the technique with a novel accelerated k-space trajectory, DW-CRT,[25] and showed its feasibility for the ^{23}Na acquisition. The simulation and phantom studies showed that the proposed technique could be used as an alternative to the slice-selective gradient approach in which achieving an ultra-short TE is difficult. On the other hand, the in-vivo study demonstrated that the proposed MRSI method could be a faster option to provide ^{23}Na-T_2* maps compared to multi-echo 3D-MRI approaches that usually require lengthy acquisition times.[7,16–20]

Although MRSI and the 3D-MRI sequences have different acquisition and reconstruction parameters, the estimated ^{23}Na spatial distributions were in a good agreement with a regression line close to unity and a small bias of 0.67 mM (Figure 7B). This variability between the two sequences results is expected due to their different spatial resolution (MRSI: 2.5 × 2.5 mm^2; 3D-MRI: 4 × 4 mm^2), and spatial response function.[25,26] Moreover, the field inhomogeneitiy correction was only performed on the MRSI reconstruction. A recent study with a similar 3D sequence, but with double echo to measure B_0 and correct for its inhomogeneity at 3T, showed a small enhancement in the results.[32]

In this work, we provided an accelerated technique to conduct voxel-wise T_2* measurements within an acceptable scan time (15 minutes) while maintaining the spatial resolution. It is worth mentioning that recently a number of studies have shown the feasibility of voxel-wise T_2* mapping in the brain using UTE-3D acquisition techniques.[16–20] However, these techniques were conducted with fewer time points (8–38 echoes), and require long acquisition times (26 min - 1 h). Moreover, many of these methods were either done with lower spatial resolution, at a higher magnetic field, or done with both. If the proposed MRSI method was applied under these conditions, further reduction in scan time can be achieved.

The estimated mean muscle relaxation times (T^*_{2Fast} = 0.7 ± 0.1 ms of F_{Fast} = 37 ± 2 %; T^*_{2Slow} = 13.2 ± 0.2 ms of F_{Slow} = 63 ± 2 %) are in line with previously reported values measured using single voxel ^{23}Na MRS (T^*_{2Fast} = 0.8 ± 0.2 [32 ± 7 %], T^*_{2Slow} = 12.4 ± 1.8 ms [68 ± 7 %]).[21] The average muscle absolute concentration (after T_2* correction) was

28.6 ± 3.3 mM, which is also in agreement with reported biopsy results.[7] In terms of T_2* spatial distribution, the slow fraction is larger and slower in areas with large blood vessel, which makes sense. In blood vessels, the motion is less restricted compared to muscles and spins move more freely that resulting in longer T_2* values and the time averaged QI is minimal, which means that the fast component fraction is also minimal.

One can conclude at least two important reasons for performing a relaxation study. First, relaxation corrected data provides a better estimation of absolute concentration. In Figure 7, the estimated concentration at 0.3 ms increased by 27% after the T_2* correction (the comparison slope increased from unity to 1.27). This enhancement in concentration (Figure 6C&7) indicates that T_2* correction might be useful for more accurate quantification results even with UTE measurements, as T_2*-corrected data showed a better agreement with biopsy results (see the preceding paragraph). Additionally, one can see that even with the UTE measurement, a relaxation bias might be present due to the difference in decay mode between the reference bottles and muscle tissue (Figure 6D). The second use of T_2* mapping is to provide extra information that can be utilized to assess potential physiological changes. However, the voxel-wise T_2 correction may result in overestimating ^{23}Na concentrations in certain regions, where partial volume effect exists. This was seen in this study within areas where the main blood vessels start bifurcating to smaller vessels (see the regions of very large difference in Figure 6C).

According to the repeatability analysis, the proposed method showed high repeatability (CV = 4%, ICC = 0.98). The repeatability CVs and ICCs after the T_2* correction were close to the 3D MRI results (CV = 5%, ICC = 0.95 vs CV = 6% and ICC = 0.89). Thus, the proposed MRSI might be a potential method to estimate the T_2* values and the absolute sodium concentration (free from T_2* bias) within a reasonable scan time. Since ^{23}Na signal suffers from low SNR, scanning with large voxels or at high fields is performed to maintain good SNR within a reasonable scan time. Compared to other techniques at 3T, the proposed MRSI method acquires 64 data points with an acceptable spatial resolution (2.5 mm^2, nominal in-plane) and acquisition time (15 minutes and 24 seconds). Since the FID data were collected at different time points with different phases, ΔB_0 correction is also feasible without extra scans. Although scanning at the isocenter reduces the effect of ΔB_0, the proposed approach can be crucial for studies conducted off the isocenter and/or at higher field strengths. Additionally, in this study, we performed the ΔB_0 correction and low-rank filtering in separate steps. Using a combined B_0-corrected low-rank filtering method is expected to improve our results.[33] Moreover, even after ΔB_0 correction, some artifact (shading across the phantoms) is still present. The potential influence of this small artifact on quantification results has been minimized by using the average signal within carefully placed ROIs that covers the entire phantom (without their walls) that reduces any potential spatial variation. This resulted in a calibration line with high linearity and allowed an excellent fitting with R^2 almost = 1 (see example in Supporting Figure S2). Thus, we believe that this artifact does not cause a major quantification issue. Additionally, to ensure a proper biexponential fitting for T_2* estimation, the prolonged acquisition sampling duration allows for acquisition of the entire FID. This is important for areas of longer T_2* values like reference phantoms.

A limitation of this method is its large dependency on the T_1 value of the scanned tissues. In order for the OVS to perform correctly, the sequence needed to be applied with TI = ln(2) × tissue's T_1 (close approximation when TR>>T_1). In this study, we used a TI of 20 ms because muscles have a ^{23}Na T_1 of 29 ms, as previously measured at 3T.[4] To suppress tissues with shorter T_1, such as cartilages, the TI has to be reduced, which may be technically challenging. However, one can make sure that no such tissues are within the active region of the receiving coil. For instance, we avoided getting residual signals from the knee by keeping it outside the ^{23}Na-coil field. Here, we evaluated the technique in healthy muscles. However, T_1 might change with diseases. Although it is expected that this OVS technique would still achieve good suppression even with slightly T_1 deviations, future studies might be needed to confirm this. In this study, no ΔB_1 correction was implemented. However, the coil B_1 mapping was performed using a GRE sequence with the double angel method.[34] Since the ΔB_1 map was very homogeneous, no ΔB_1 correction was conducted. The ^{23}Na-coil ΔB_1 map can be found in Supporting Figure S3. Although the sample size may be a limitation in this study, there is no reason to anticipate a large difference in our results with larger sample size.

For this study, we used a volume coil placed along the z-axis of the scanner. Thus, the spatial B_1 variation is expected to increase along the z-direction, where the OVS bands are applied. Together with inversion pulses, OVS bands make the reduction of the longitudinal magnetization depends mainly on the T_1 and is independent of spatial B_1 variations. Additionally, the broad-BW OVS pulses were applied with a B_1 peak of 29 μT, 2.56 ms duration, and a thickness of 100 mm that resulted in no SAR issues.

The considerable regional variability within T_2*, their fraction maps, and the increased accuracy of concentration maps demonstrate the potential for future characterization of ^{23}Na in conditions such as muscle diseases, diabetes, cancers, strokes, cartilage degeneration, and to evaluate physiological interventions. The reduction in scan time will increase the technique's availability and reduce motion artifacts. Technically, while still using a long enough TR (4–5 times T_1), a shorter TR than that used in this study can be used, which will accelerate the acquisition further. In addition to ensuring a full T_1 recovery and maintaining a low SAR, we used a very long TR because we wanted to study the existence of any long decaying species. However, no such decay has been noticed within the scanned area. Thus, we would suggest using a TR of about half of the value used here. Additionally, scanning with shorter TEs, and with higher sampling frequency could enhance the fitting quality further. Beyond ^{23}Na, the proposed MRSI technique might be useful for ^{1}H applications such as imaging dental tissues,[35] which characterized by a very fast T_2*. Measurements of other fast decaying nuclei such as ^{13}C, ^{31}P, or ^{15}N may benefit from the proposed technique as well.

5 | CONCLUSIONS

The proposed method allows fast data collection for measuring in vivo sodium concentrations and T_2* values at high reliability. This may facilitate evaluating pathological and physiological changes related to the ^{23}Na concentration and T_2* values within a clinically feasible time, and with a good spatial resolution at 3T.

Supplementary Material

Refer to Web version on PubMed Central for supplementary material.

ACKNOWLEDGMENTS

The study was supported by the Indiana CTSI and funded in part by grant #UL1TR001108 from the NIH, NCATS, CTS Award, as well as a pilot grant by the College of Health and Human Sciences, Purdue University.

Funding information

Indiana CTSI; grant #UL1TR001108 from the NIH, NCATS, CTS Award; as well as a pilot grant by the College of Health and Human Sciences, Purdue University.

REFERENCES

1. Madelin G, Lee JS, Regatte RR, Jerschow A. Sodium MRI: Methods and applications. Prog Nucl Magn Reson Spectrosc. 2014. doi:10.1016/j.pnmrs.2014.02.001
2. Kopp C, Linz P, Dahlmann A, et al. 23Na magnetic resonance imaging-determined tissue sodium in healthy subjects and hypertensive patients. Hypertension. 2013. doi:10.1161/HYPERTENSIONAHA.111.00566
3. Kopp C, Linz P, Maier C, et al. Elevated tissue sodium deposition in patients with type 2 diabetes on hemodialysis detected by 23Na magnetic resonance imaging. Kidney Int. 2018. doi:10.1016/j.kint.2017.11.021
4. Nagel AM, Amarteifio E, Lehmann-Horn F, et al. 3 Tesla sodium inversion recovery magnetic resonance imaging allows for improved visualization of intracellular sodium content changes in muscular channelopathies. Invest Radiol. 2011. doi:10.1097/RLI.0b013e31822836f6
5. Weber MA, Nielles-Vallespin S, Essig M, Jurkat-Rott K, Kauczor HU, Lehmann-Horn F. Muscle Na + channelopathies: MRI detects intracellular 23Na accumulation during episodic weakness. Neurology. 2006. doi:10.1212/01.wnl.0000233841.75824.0f
6. Schepkin VD, Chenevert TL, Kuszpit K, et al. Sodium and proton diffusion MRI as biomarkers for early therapeutic response in subcutaneous tumors. Magn Reson Imaging. 2006. doi:10.1016/j.mri.2005.12.004
7. Constantinides CD, Gillen JS, Boada FE, Pomper MG, Bottomley PA. Human skeletal muscle: Sodium MR imaging and quantification - Potential applications in exercise and disease. Radiology. 2000. doi:10.1148/radiology.216.2.r00jl46559
8. Bansal N, Szczepaniak L, Ternullo D, Fleckenstein JL, Malloy CR. Effect of exercise on 23Na MRI and relaxation characteristics of the human calf muscle. J Magn Reson Imaging. 2000. doi:10.1002/(sici)1522-2586(200005)11:5<532::aid-jmri9>3.3.co;2-r
9. Berendsen HJC, Edzes HT. THE OBSERVATION AND GENERAL INTERPRETATION OF SODIUM MAGNETIC RESONANCE IN BIOLOGICAL MATERIAL. Ann N Y Acad Sci. 1973. doi:10.1111/j.1749-6632.1973.tb30799.x
10. Rooney WD, Springer CS. A comprehensive approach to the analysis and interpretation of the resonances of spins 3/2 from living systems. NMR Biomed. 1991. doi:10.1002/nbm.1940040502
11. Boada FE, Christensen JD, Huang-Hellinger FR, Reese TG, Thulborn KR. Quantitative in vivo tissue sodium concentration maps: The effects of biexponential relaxation. Magn Reson Med. 1994. doi:10.1002/mrm.1910320210
12. Ra JB, Hilal SK, Cho ZH. A method for in vivo MR imaging of the short T2 component of sodium-23. Magn Reson Med. 1986. doi:10.1002/mrm.1910030213
13. Nagel AM, Bock M, Hartmann C, et al. The potential of relaxation-weighted sodium magnetic resonance imaging as demonstrated on brain tumors. Invest Radiol. 2011. doi:10.1097/RLI.0b013e31821ae918
14. Bottomley PA. Sodium MRI in Man: Technique and Findings. In: Encyclopedia of Magnetic Resonance. ; 2012. doi:10.1002/9780470034590.emrstm1252

15. Kratzer FJ, Flassbeck S, Nagel AM, et al. Sodium relaxometry using 23Na MR fingerprinting: A proof of concept. Magn Reson Med. 2020. doi:10.1002/mrm.28316
16. Blunck Y, Josan S, Taqdees SW, et al. 3D-multi-echo radial imaging of 23Na (3D-MERINA) for time-efficient multi-parameter tissue compartment mapping. Magn Reson Med. 2018. doi:10.1002/mrm.26848
17. Riemer F, Solanky BS, Wheeler-Kingshott CAM, Golay X. Bi-exponential 23Na T2* component analysis in the human brain. NMR Biomed. 2018. doi:10.1002/nbm.3899
18. Lommen JM, Flassbeck S, Behl NGR, et al. Probing the microscopic environment of 23 Na ions in brain tissue by MRI: On the accuracy of different sampling schemes for the determination of rapid, biexponential T2* decay at low signal-to-noise ratio. Magn Reson Med. 2018. doi:10.1002/mrm.27059
19. Ridley B, Nagel AM, Bydder M, et al. Distribution of brain sodium long and short relaxation times and concentrations: a multi-echo ultra-high field 23Na MRI study. Sci Rep. 2018. doi:10.1038/s41598-018-22711-0
20. Syeda W, Blunck Y, Kolbe S, Cleary JO, Johnston LA. A continuum of T2* components: Flexible fast fraction mapping in sodium MRI. Magn Reson Med. 2019. doi:10.1002/mrm.27659
21. Gerhalter T, Carlier PG, Marty B. Acute changes in extracellular volume fraction in skeletal muscle monitored by 23Na NMR spectroscopy. Physiol Rep. 2017. doi:10.14814/phy2.13380
22. Gerlach DA, Schopen K, Linz P, et al. Atrophy of calf muscles by unloading results in an increase of tissue sodium concentration and fat fraction decrease: a 23Na MRI physiology study. Eur J Appl Physiol. 2017. doi:10.1007/s00421-017-3647-4
23. Choi IY, Tkac I, Gruetter R. Single-shot, three-dimensional “non-echo” localization method for in vivo NMR spectroscopy. Magn Reson Med. 2000. doi:10.1002/1522-2594(200009)44:3<387::AID-MRM8>3.0.CO;2-3
24. Henning A, Fuchs A, Murdoch JB, Boesiger P. Slice-selective FID acquisition, localized by outer volume suppression (FIDLOVS) for 1H-MRSI of the human brain at 7 T with minimal signal loss. NMR Biomed. 2009. doi:10.1002/nbm.1366
25. Chiew M, Jiang W, Burns B, et al. Density-weighted concentric rings k-space trajectory for1H magnetic resonance spectroscopic imaging at 7 T. NMR Biomed. 2018. doi:10.1002/nbm.3838
26. Nagel AM, Laun FB, Weber MA, Matthies C, Semmler W, Schad LR. Sodium MRI using a density-adapted 3D radial acquisition technique. Magn Reson Med. 2009. doi:10.1002/mrm.22157
27. Fessler JA, Sutton BP. Nonuniform fast Fourier transforms using min-max interpolation. IEEE Trans Signal Process. 2003. doi:10.1109/TSP.2002.807005
28. Gast LV, Henning A, Hensel B, Uder M, Nagel AM. Localized B0 shimming based on 23Na MRI at 7 T. Magn Reson Med. 2020. doi:10.1002/mrm.28011
29. Sutton BP, Noll DC, Fessler JA. Fast, iterative image reconstruction for MRI in the presence of field inhomogeneities. IEEE Trans Med Imaging. 2003. doi:10.1109/TMI.2002.808360
30. Nguyen HM, Peng X, Do MN, Liang ZP. Denoising MR spectroscopic imaging data with low-rank approximations. IEEE Trans Biomed Eng. 2013. doi:10.1109/TBME.2012.2223466
31. Jackson JI, Meyer CH, Nishimura DG, Macovski A. Selection of a Convolution Function for Fourier Inversion Using Gridding. IEEE Trans Med Imaging. 1991. doi:10.1109/42.97598
32. Gerhalter T, Gast LV, Marty B, Uder M, Carlier PG, Nagel AM. Assessing the variability of 23Na MRI in skeletal muscle tissue: Reproducibility and repeatability of tissue sodium concentration measurements in the lower leg at 3 T. NMR Biomed. 2020. doi:10.1002/nbm.4279
33. Liu Y, Ma C, Clifford B, Lam F, Johnson CL, Liang ZP. Field-inhomogeneity-corrected low-rank filtering of magnetic resonance spectroscopic imaging data. In: 2014 36th Annual International Conference of the IEEE Engineering in Medicine and Biology Society, EMBC 2014. ; 2014. doi:10.1109/EMBC.2014.6945098
34. Stollberger R, Wach P. Imaging of the active B1 field in vivo. Magn Reson Med. 1996. doi:10.1002/mrm.1910380225
35. Stumpf K, Rasche V, Kaye E, Pauly JM. Two-dimensional UTE overview imaging for dental application. Magn Reson Med. 2020. doi:10.1002/mrm.28312

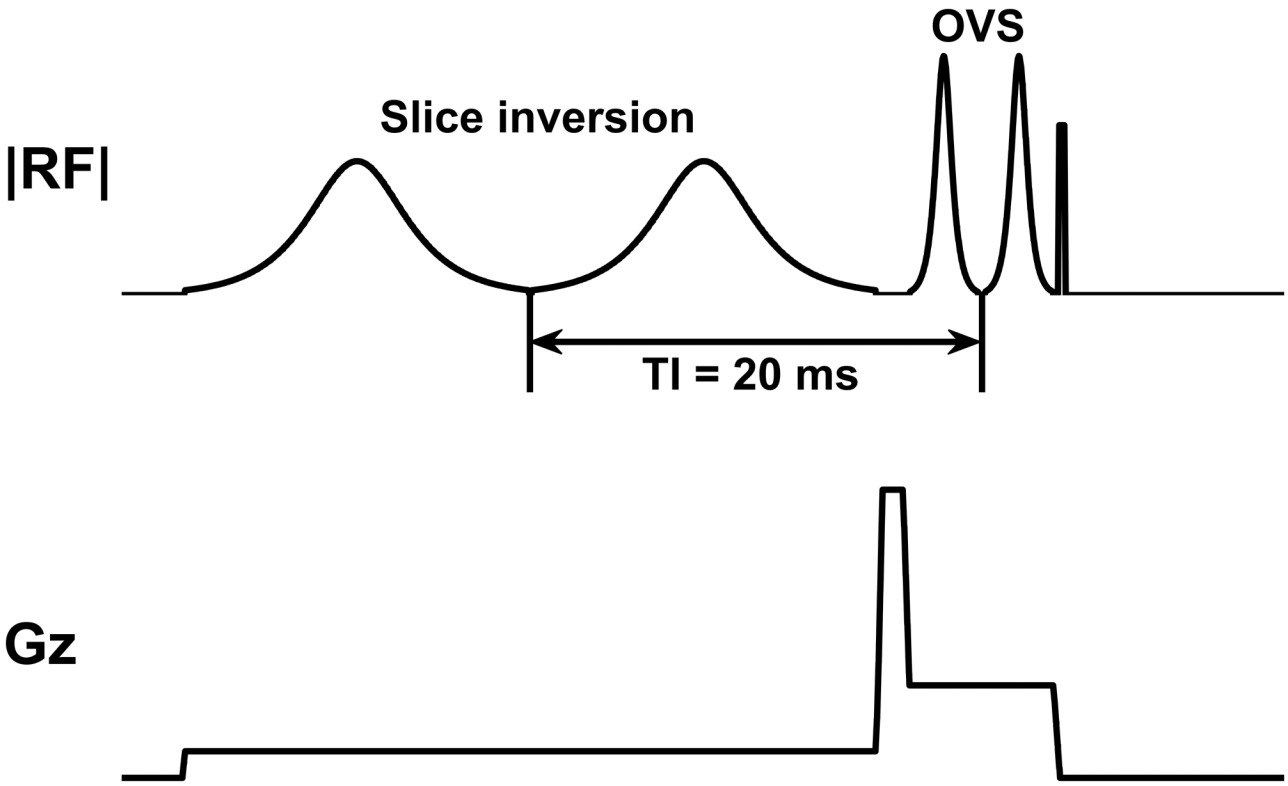

FIGURE 1.

Pre-readout MRSI pulse sequence. To suppress the unwanted region outside the slice of interest (SOI), two OVS bands are assigned before the FID excitation. These OVS bands along the z-direction are applied after two selective 180° inversion recovery pulses covering the area outside the SOI at inversion time (TI) = ln(2) × 29 ms = 20 ms, where 29 ms is the T_1 of muscles.[4] Directly after the OVS band pulses, a nonselective 90° excitation pulse is applied before starting the FID-MRSI readout

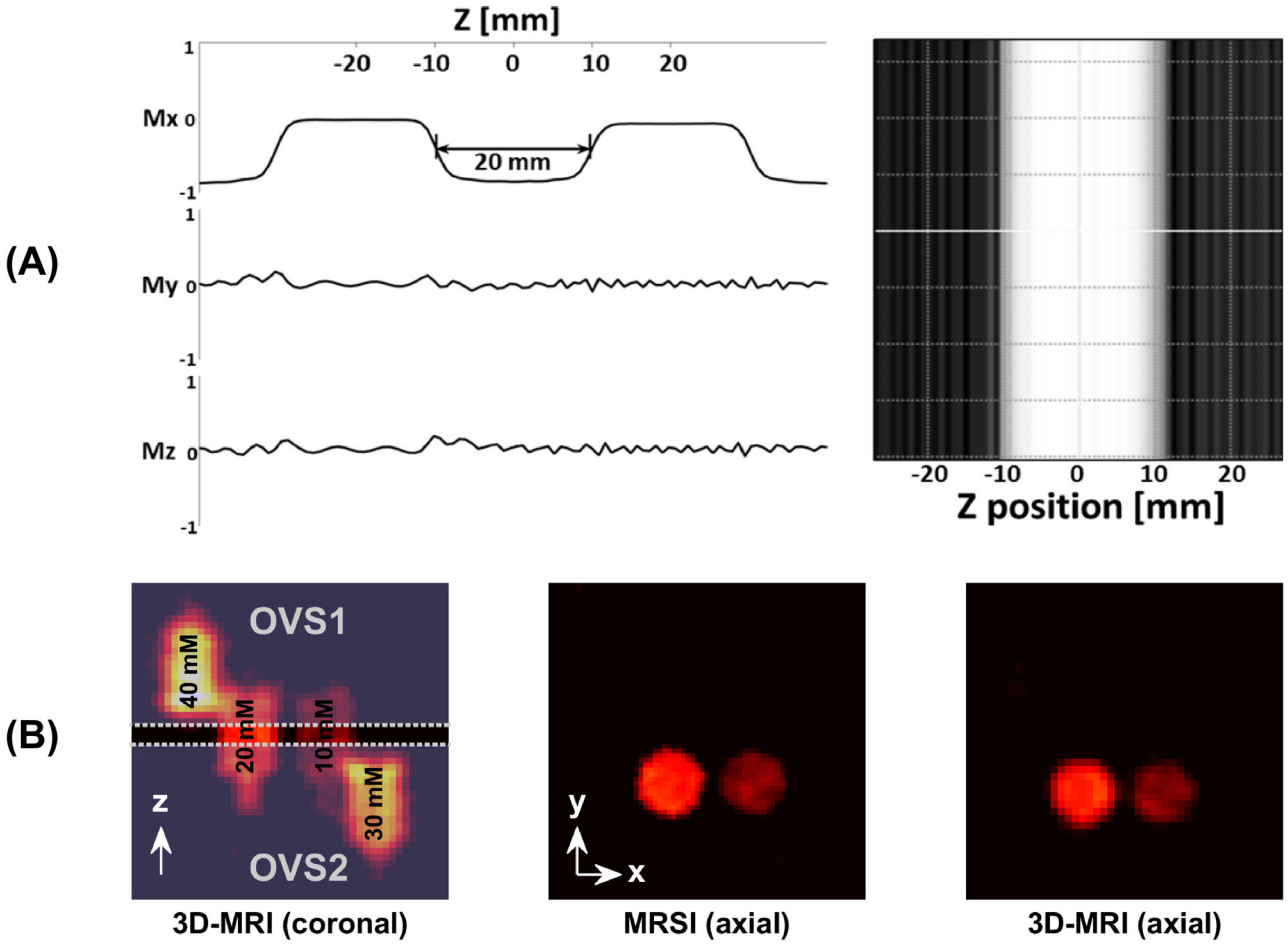

FIGURE 2.

SIRENE-MRSI localization performance evaluation by simulation and phantom studies. A, Simulated data showing a sharp spatial profile along the z-direction when using an inversion time of 20 ms. B, Phantom evaluation of the OVS localization. Two ^{23}Na phantoms (10 and 20 mM) were placed at the center of the slice of interest (SOI), which were located between the 2 OVS bands. Two additional phantoms of higher concentrations (30 and 40 mM) were placed outside the SOI, within the OVS bands. As shown in the axial images, the MRSI signal is obtained only from the phantoms within the SOI, resulting in an image that is very similar to that produced by the 3D-MRI sequence

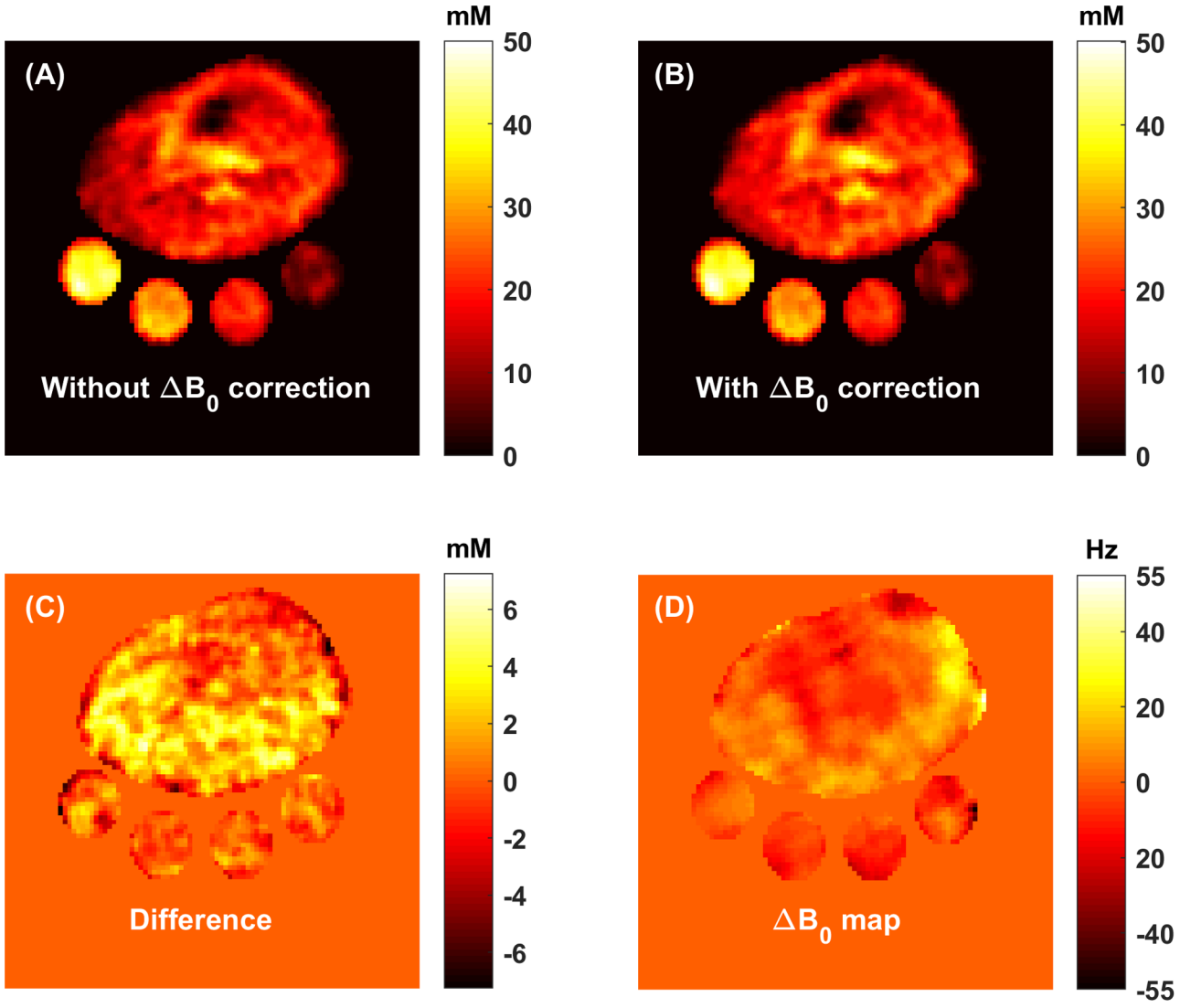

FIGURE 3.

A, An example of a ^{23}Na-MRSI map without ΔB_0 correction. B, The same ^{23}Na-MRSI map with ΔB_0 correction. C, The difference in concentration resulted from applying the ΔB_0 correction. D, ^{23}Na-ΔB_0 map used to correct the ^{23}Na map

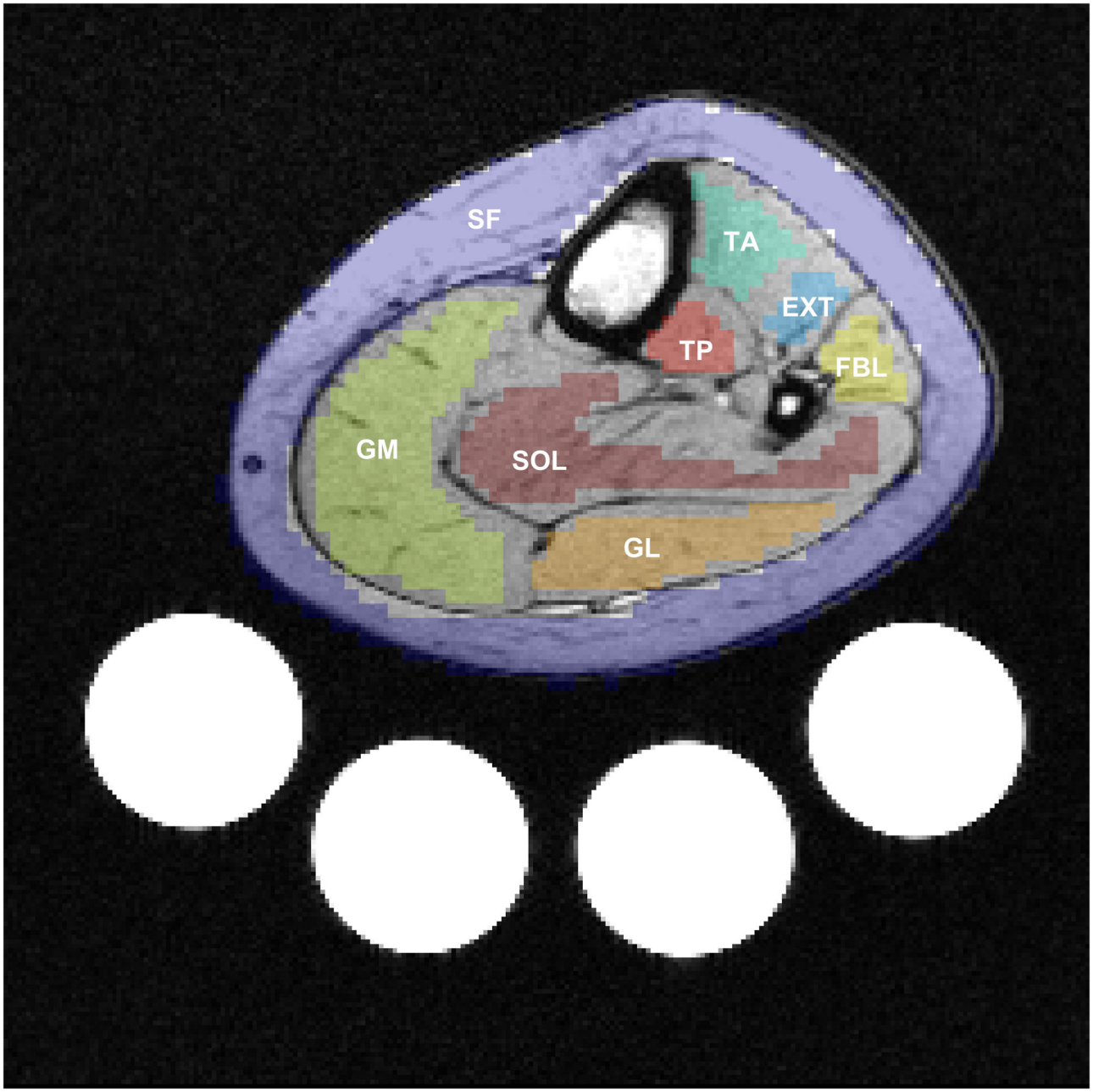

FIGURE 4.

Representative segmented regions of interest (ROIs). Calf muscle and subcutaneous fat (SF) ROIs were drawn based on their high-resolution T1 axial ^{1}H-image, which allows clear anatomical features for segmentation. Seven ROIs were drawn to cover the main human calf muscles: SOL, Soleus; FBL, Fibularis; EXT, Extensor longus; TA, Tibialis anterior; GM, Gastrocnemius medialis; GL, Gastrocnemius lateralis; and TP, Tibialis posterior muscles. The shown ROIs are presented in the MRSI resolution and overlaid over their corresponding high-resolution T1 anatomical image

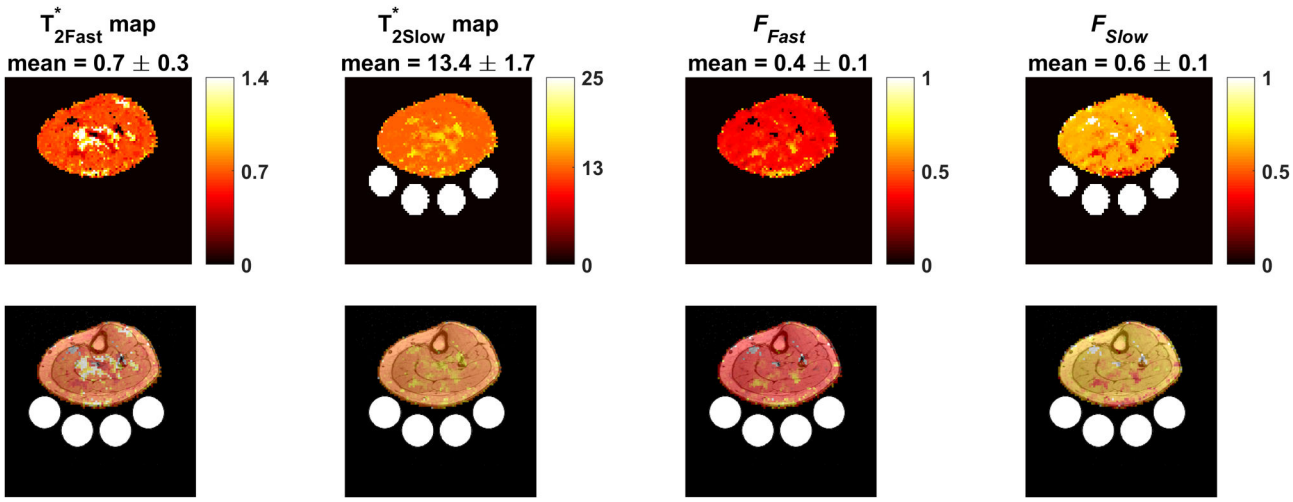

FIGURE 5.

Representative relaxation maps. Top panel: fast and slow T_2* maps, and their corresponding signal fraction (F_{Fast}, and F_{Slow}). Their mean values from the entire leg slice (without the bottles) are listed above their maps. Bottom panel: the same maps overlaid on their anatomical images

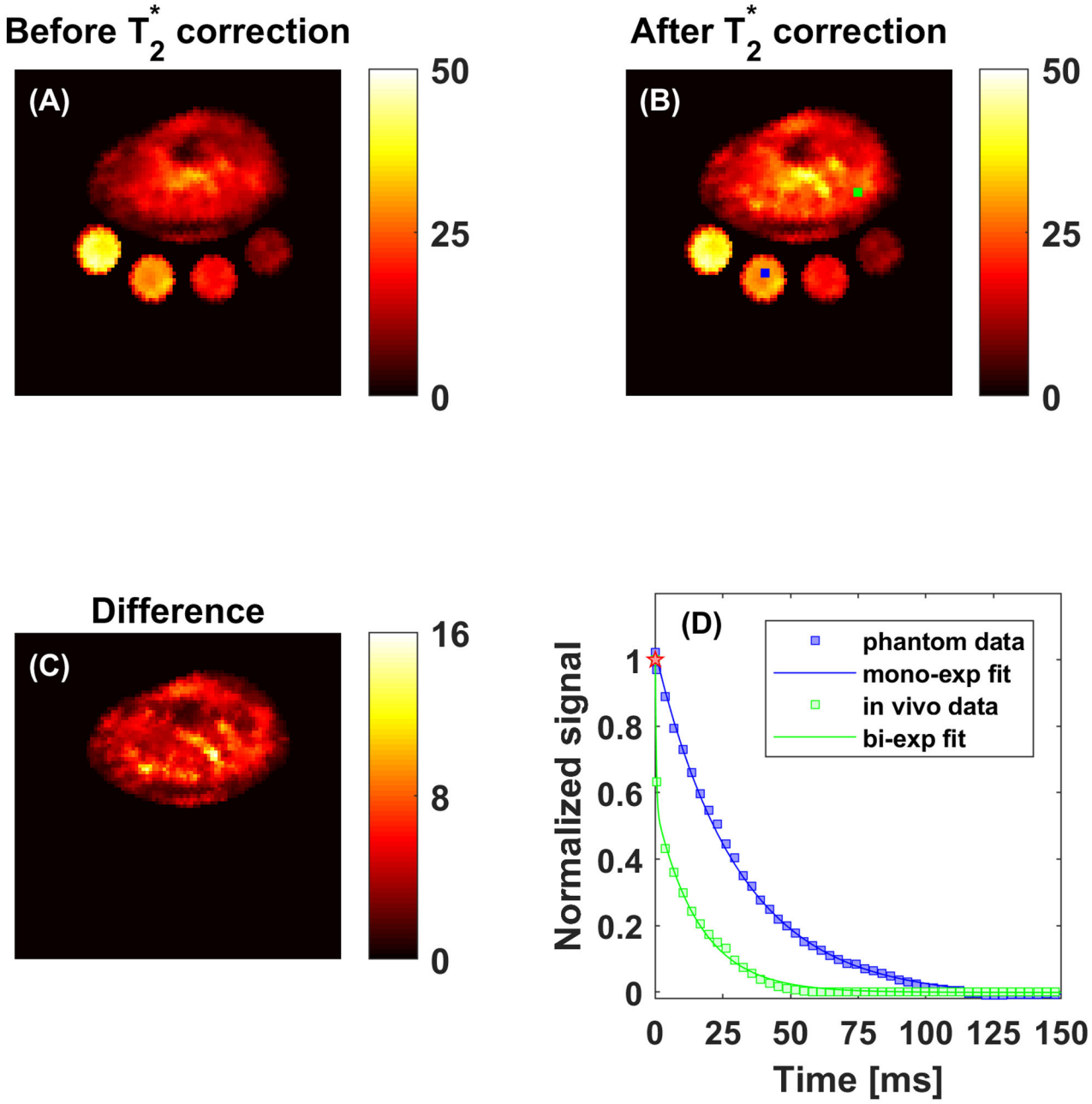

FIGURE 6.

Illustrations of the importance of the relaxation correction. The difference between the data acquired at 0.55 ms (A) and the data after correction (B), shows a large improvement in concentration estimation. In the difference map (C), about 5 mM difference in muscles was found. (The red star, D) represents the spin density-weighted signal (≈ the initial signal before decay) corresponding to 30 mM absolute concentration. The fitting example of leg voxel (2.5 × 2.5 mm^2 green box, B and D) and quantification reference voxel (2.5 × 2.5 mm^2 blue box, B and D) with this absolute concentration shows how their signal can diverge with time before fully decaying. Such diverging can result in T_2*-weighted signals across the FOV with time, leading to underestimated quantification results

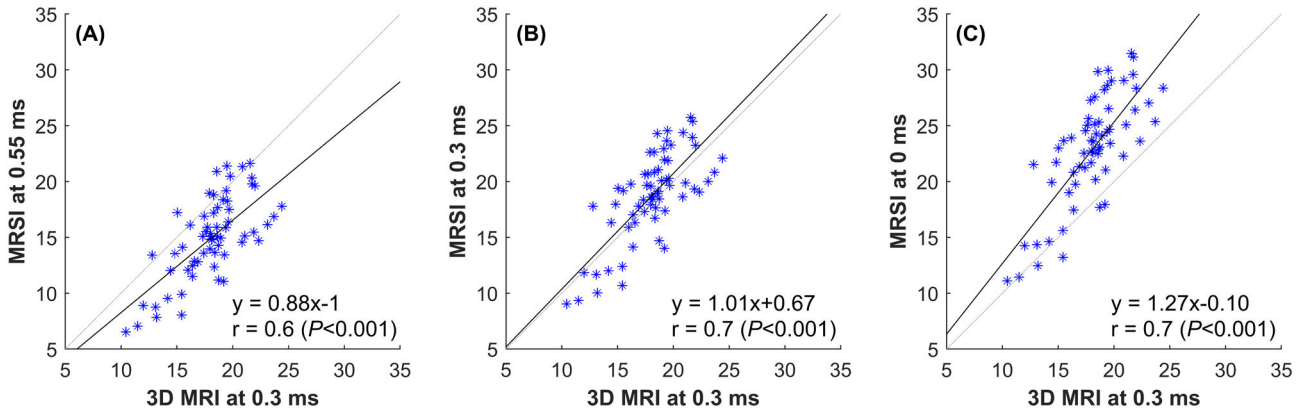

FIGURE 7.

Results of the regression analysis comparing the normalized mean signal (normalized to the phantom signal) of the MRSI and the 3D MRI within 64 regions of interest from all subjects data (7 muscles and one subcutaneous fat ROIs × 4 subjects × 2 scans). A, MRSI data before T_2* correction (at 0.55 ms) compared to the 3D-MRI data. B, The MRSI data extrapolated (based on the estimated T_2* values) to represent data at 0.3 ms compared to the 3D-MRI data, which was acquired at TE = 0.3 ms. The regression line almost matches the unity line (slope ≈1). C, Comparing MRSI data after T_2* correction to the 3D-MRI data. The increase in slope (from A to C) represents the T_2* correction impact

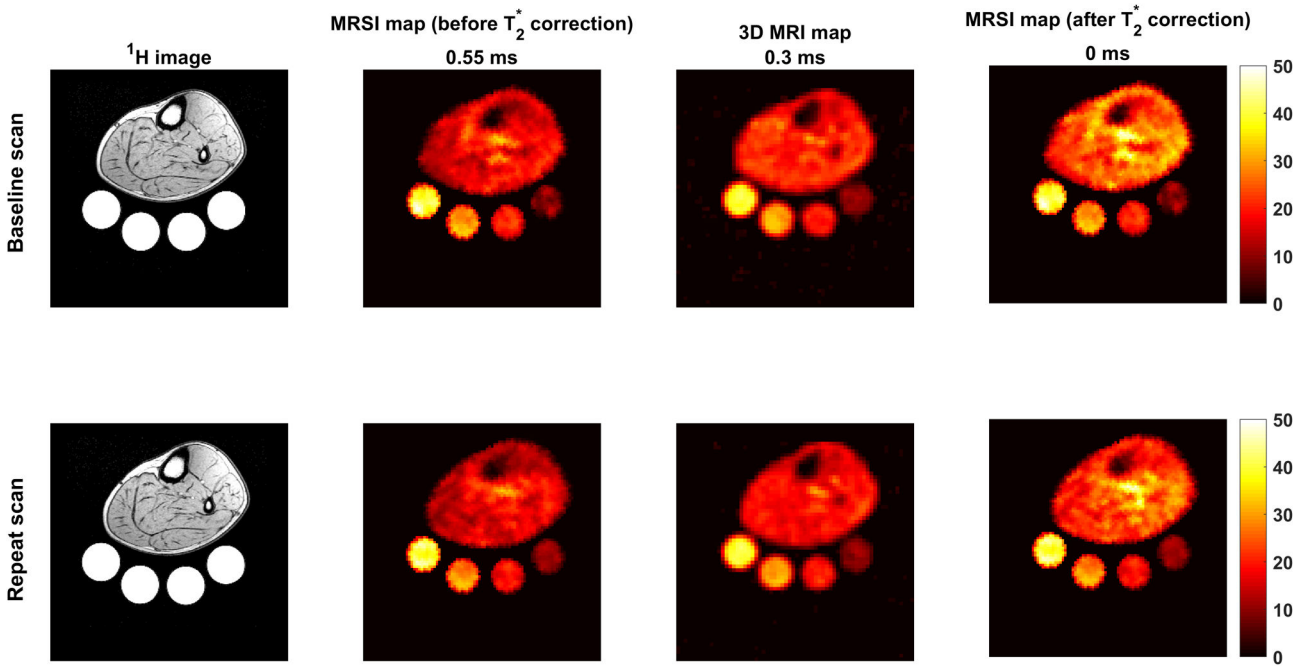

FIGURE 8.
Data example of baseline and repeat scans

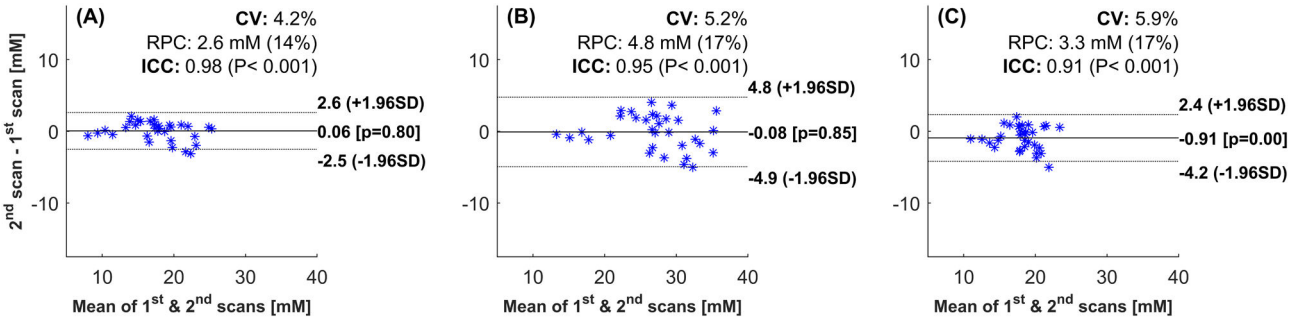

FIGURE 9.

Evaluation of repeatability by Bland–Altman analysis. A, The results from the MRSI data before T_2* correction. B, The results from the MRSI data after the T_2* correction. C, The 3D-MRI data results. The graphs represent the variability of the measured data (muscles and subcutaneous fat ROIs from all subjects, 7 muscles and one subcutaneous fat ROIs × 4 subjects) between 1st and 2nd scans. The coefficient of variation (CV), reproducibility coefficient (RPC), systematic bias, and intraclass correlation coefficient (ICC) values are listed on each plot

TABLE 1

Regions of interest absolute ^{23}Na concentration, T_2* values, and signal fractions

ROI	Concentration [mM]	T^*_{2Fast} [ms]	F_{Fast} [%]	T^*_{2Slow} [ms]	F_{Slow} [%]
SF	15.7 ± 1.9	0.71 ± 0.04	38.9 ± 1.5	13.2 ± 0.1	61.1 ± 1.5
GM	25.0 ± 2.8	0.67 ± 0.03	38.3 ± 2.1	13.2 ± 0.4	61.7 ± 2.1
TA	25.3 ± 2.1	0.61 ± 0.09	34.9 ± 2.1	12.9 ± 0.4	65.0 ± 2.1
EXT	26.9 ± 3.5	0.62 ± 0.19	35.8 ± 2.8	13.0 ± 0.5	64.2 ± 2.8
GL	28.6 ± 3.1	0.73 ± 0.06	38.6 ± 0.9	13.1 ± 0.2	61.4 ± 0.9
TP	29.5 ± 2.3	0.73 ± 0.21	37.8 ± 3.4	13.3 ± 0.5	62.2 ± 3.4
FBL	31.1 ± 3.4	0.59 ± 0.14	34.8 ± 2.8	13.3 ± 0.6	65.2 ± 2.8
SOL	34.1 ± 2.2	0.76 ± 0.11	38.4 ± 2.8	13.3 ± 0.4	61.6 ± 2.8
Phantom	10 – 40	---	---	29.5 ± 0.3	100.0

Abbreviations: SF, Subcutaneous fat; GM, Gastrocnemius medialis muscle; TA, Tibialis anterior muscle; EXT, Extensor longus muscles; GL, Gastrocnemius lateralis muscle; TP, Tibialis posterior muscle; FBL, Fibularis muscles; SOL, Soleus muscle. F_{Fast}, The fraction of fast decaying signal; F_{Slow}, The fraction of slow decaying signal.